Influence of Discretisation on Stiffness and Failure Prediction in Crashworthiness Simulation of Automotive High Pressure Die Cast Components

Authors: Felix Brenner[1], Michael Buckley[2], Helmut Gese[1], Gernot Oberhofer[1]

(1) MATFEM Partnerschaft Dr. Gese & Oberhofer, Munich, Germany
(2) Jaguar Land Rover Limited, Gaydon, United Kingdom

1 Introduction

1.1 Problem description

Castings are widely used as part of the car chassis in automobile manufacture because of their light weight and the flexibility of the design process. Due to the comparable low ductility of castings, it is essential for crash simulations to gain dependable analyses. However, modelling casting parts correctly for finite element analyses is an issue for several reasons. In order to represent the elastoplastic stiffness correctly and thus to obtain reliable failure predictions, an accurate prediction of plastic strains and the corresponding stress states is required. To meet these conditions an adequate material and failure model is needed. Besides the characterisation and modelling of the material, the geometric discretisation is a trade-off between computational costs, meshing effort and the quality of the results that can be achieved in simulations. Typically, no general guidance is provided on the appropriate element formulation or the impact this choice may have on the results. Lastly, in industrial environments economic competition usually does not allow for extensive basic research. Conservative methodologies in development and simulation of castings are the norm since new methods carry the risk of failure. Thus avenues of improving accuracy and reducing costs of simulations remain to be explored.

1.2 Course of action

A concise introduction on material modelling for crash simulations with the material model MF GenYld+CrachFEM® in chapter 2 provides information about the defined elastoplastic and failure behaviour. After this revision of theoretical background the findings of an elastoplastic buckling test which was performed first to outline accuracy and efficiency of different element types and formulations in the FEA code LS-DYNA® are presented. For reasons of brevity, only the most important findings for the subsequent tests are given. Only element formulations that performed well in this buckling study are considered in the following investigations. With regard to fracture prediction, a generic model of a specimen subjected to a complex stress state is expected to show the capability of relevant element types and effects induced by discretisation. Finally, findings of the basic tests are incorporated and simulations of the component under testing conditions are performed. The results are assessed considering their quality, efficiency and agreement with experimental outcome. The aim of the work is to find the most efficient way to model castings in general and to implement the findings on an automotive component, validating the results of finite element simulations against experiments. In doing so, the focus is not on fitting results of analyses according to tests, but on identifying sources of influence, rating them and thus obtaining a profound understanding of methodically modelling castings.

2 Material modelling

2.1 Elasto-plastic behaviour

The elastic regime of aluminium castings is typically considered to be isotropic as the production process leads to randomly oriented grains without a preferred direction [1].
Several yield conditions exist, defining the onset of plastic flow. Besides the isotropic von Mises yield locus, a number of orthotropic yield conditions are available in MF GenYld+CrachFEM. Different yield

© 2013 Copyright by Arup

stresses can be found in some aluminium casting alloys for tension and compression (strength difference effect). To account for such phenomena, MF GenYld offers the option to modify given yield loci at specific stress states and thus correcting deviations of the yield strength from the basic yield locus, see [2]. For the description of the used alloy, a modified von Mises yield locus is used with asymmetry in tension and compression.
The hardening behaviour is described by a Ghosh hardening law, which accorded best with experimental tests performed to derive material properties. The strain rate dependent hardening behaviour of the alloy is taken into account, Fig. 1.

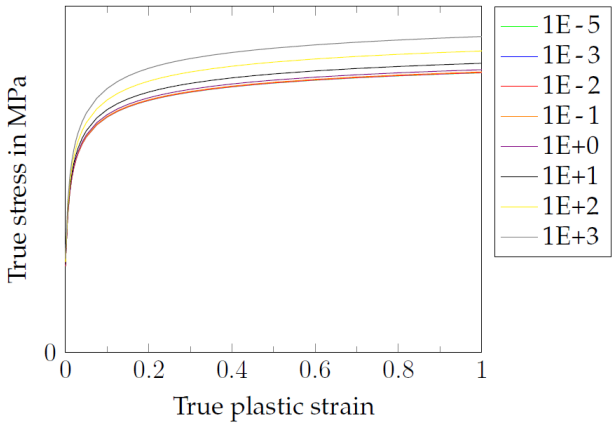

Fig. 1: Analytical approximation of strain rate dependent hardening in uniaxial tension for Al-HPDC, rates in s^{-1} [3]

2.2 Failure criteria

The failure mechanisms observed in aluminium alloys are ductile normal fracture, ductile shear fracture and localised necking followed by one of the previously named fracture mechanisms. Localised necking is an instability that emerges from local inhomogenities, respectively. Due to small plastic strains up to fracture, for the failure of cast components, localised necking is usually not the most critical failure mechanism, but one of the other two fracture mechanisms mentioned above. Nevertheless, instability followed by localised necking can be observed in some ductile aluminium casting alloys.

In CrachFEM there are two different ductile fracture mechanisms, both leading to separate fracture strains. The one which yields the lower value for a specific stress state will lead to fracture. Thus, a criterion that is based on the predominant physical effects causing failure is introduced. In the following the models are described according to [4], starting with the fracture model for ductile normal and ductile shear fracture.

2.2.1 Ductile normal fracture

For a plane stress state, the stress triaxiality η is sufficient to describe the stress state uniquely. It is defined according to

$$\eta = \frac{I_1}{\sqrt{3J_2}} = \frac{3\,\sigma_{hyd}}{\sigma_{vM}}. \tag{1}$$

For three-dimensional problems a parameter defining the stress state is needed as the latter one is not uniquely defined solely by the stress triaxiality η. Introducing the ratio σ_1/σ_{vM} of the maximum principal stress σ_1 and the von Mises stress σ_{vM} and merging this stress parameter with the stress triaxiality η according to

$$\beta = \beta\left(\frac{\sigma_1}{\sigma_{vM}}, \eta\right) = \frac{1 - s_{nf}\eta}{\sigma_1/\sigma_{vM}}, \tag{2}$$

© 2013 Copyright by Arup

a single stress state parameter β is defined that uniquely correlates equivalent plastic strain at fracture with a stress state. However, the parameter s_{nf} in (2) is material dependent. Using the stress state parameter β, the ductile normal fracture curve is approximated by (3) which contains the two material dependent parameters d and q

$$\varepsilon_{eq}^{**} = d\exp(-q\beta) \ . \tag{3}$$

Fig. 2 shows the approximated curves that are used to describe normal fracture in the shocktower material.

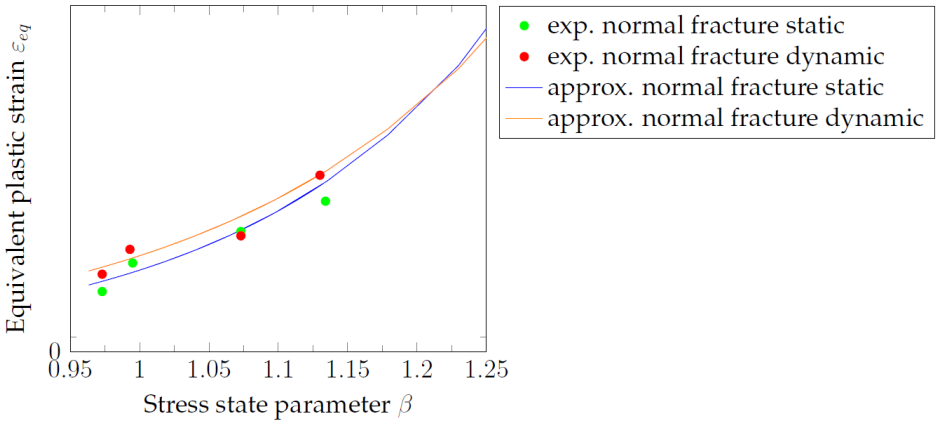

Fig. 2: Approximated normal fracture curves and experimental results for Al-HPDC [3]

2.2.2 Ductile shear fracture

Analogous to the second stress state parameter σ_1/σ_{vM} in the ductile normal fracture model, the shear fracture model uses $\tau_{\max}/\sigma_{vM}$ as a second parameter in the stress space

$$\phi = \frac{\tau_{\max}}{\sigma_{vM}} = \frac{\sigma_1 - \sigma_3}{2\sigma_{vM}}. \tag{4}$$

Again a mapping of the two stress state parameter η and ϕ on a single parameter θ is used, according to

$$\theta = \frac{1 - k_{sf}\eta}{\phi} \tag{5}$$

where k_{sf} is a material dependent parameter.
As the model already contains two independent stress state parameters, it can be applied to both plane stress and three-dimensional problems. As this general form must also be applicable to the specific case of equibiaxial tension and compression, both theoretically independent from the orientation, the following conditions must be fulfilled

$$\varepsilon_{sf}^{+} = \varepsilon_{eq}^{**}(\theta = \theta^{+}) \ , \qquad \varepsilon_{sf}^{-} = \varepsilon_{eq}^{**}(\theta = \theta^{-}) \tag{6}$$

where θ^{+} and θ^{-} denote the stress state at equibiaxial tension and compression, respectively. Using the constant parameters ε_{sf}^{+}, ε_{sf}^{-} and an orientation dependent parameter f, the analytical expression of the shear fracture model is obtained by

$$\varepsilon_{eq}^{**} = \frac{\varepsilon_{sf}^{+}\sinh(f(\theta^{-} - \theta)) + \varepsilon_{sf}^{-}\sinh(f(\theta^{+} - \theta))}{\sinh(f(\theta^{+} - \theta^{-}))}. \tag{7}$$

According to [4], the assumption that f is constant is acceptable as shear fracture is typically isotropic.

The fracture curves that result from approximation with the above equations are given in Fig. 3.

© 2013 Copyright by Arup

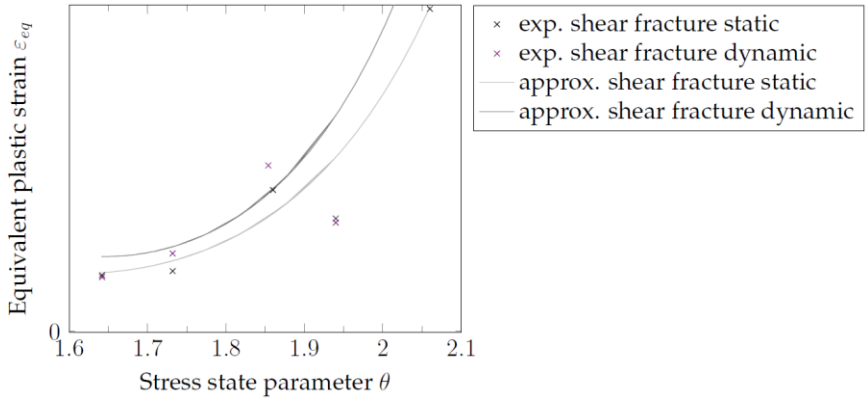

Fig. 3 : Approximated shear fracture curves and experimental results for Al-HPDC [3]

2.2.3 Localised necking

As shell elements are not able to resolve a localized neck, the algorithm Crach is used as a submodel in CrachFEM. This submodel is explained in detail in [4], but not discussed here as localised necking is of minor importance for castings.

2.2.4 Damage accumulation

In linear load cases the equivalent plastic strain at the onset of fracture can easily be derived from a fracture diagram taking the constant stress state into account. For nonlinear load cases a more general, integral calculation of the equivalent plastic strain at fracture is necessary [5]. However, this approach is not suitable for load reversals like tension-compression or torsion about an angle of $+\omega$ followed by torsion about the same axis with $-\omega$. Here a simple integral criterion with scalar description of damage yields no increase in the equivalent plastic strain for the reverse direction accompanied by a higher fracture risk. Yet, this is what can be found experimentally, which is why a tensorial fracture criterion is necessary to account for those effects as well. In the latter one a directed load does not only cause an increase of the failure risk corresponding to the loading direction but also introduces a higher rate of degradation for all orientations. Thus a reduced load capacity for the second, reversed load is attained. Such a tensorial criterion for damage accumulation is implemented in CrachFEM, but not discussed in detail here.

3 Basic studies on element performance

3.1 Buckling test

3.1.1 Modelling

Buckling under compression is a common deformation of wall sections in casting parts and a plane strain state is often encountered due to the finite wall thickness compared to the total dimension of the part. The comparatively small plastic strains that are reached before failure necessitate a precise representation of the elastoplastic deformation and the stress state.

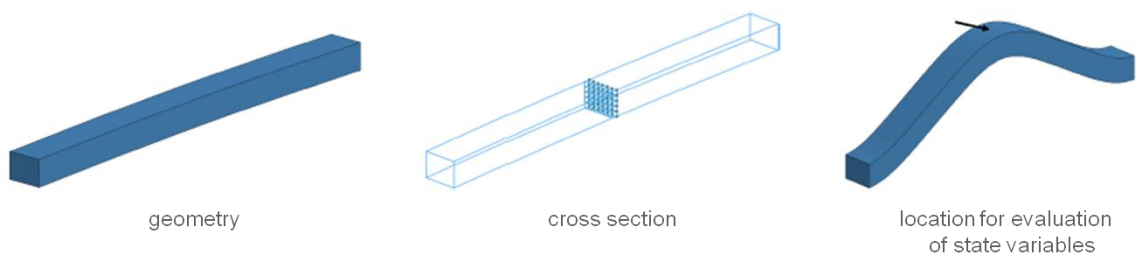

Fig. 4: Model for buckling test

The model's dimensions are shown in Fig. 4. Also, a small imperfection was put on the geometry to obtain a defined direction for buckling under compression.

© 2013 Copyright by Arup

The model was loaded by a prescribed motion at one end tip of the specimen while the other end was fixed. On both ends the transverse strain was permitted to achieve identical boundary conditions between thin shell and solid models. Left and right faces were put under plane strain condition to account for the out of plane dimensions in real parts. The velocity of the moved end tip was ramped up linearly in 5 ms. From then on it remained constant at 500 mm/s. No velocity scaling factor was applied, which means that the simulated speed corresponded to a rapid deformation as encountered in a crash.

3.1.2 Results

Tetrahedrons**:** The quadratic 10-noded tetrahedron, type 16, with 4 integration points showed superior behaviour in stiffness and accuracy of integration point variables compared with the fine hexahedron reference model. In contrast to other tetrahedrons, deviations were smaller with two elements over thickness. Even with an unreasonable coarse mesh (for an elastoplastic simulation) of only one element through thickness, the error in force-deflection was still acceptable in contrast to both the quadratic 4-noded tetrahedron, type 4, and the bilinear 10-noded composite tetrahedron, type 17, which showed remarkable locking.

Thin shells: The elastoplastic response of the thin shell models showed a very good accordance with the reference results of the hexahedron model. There was no distinct difference in quality between the underintegrated shell elements 1 and 2 and the fully integrated shell, type 16, for this load case. Comparing different mesh densities revealed that all shells suffered from bad aspect ratios, that is, if the thickness was of the same size the other dimensions were. While the deviation in force-deflection did not become unacceptably high, plastic strains and failure risk were clearly overestimated.

3.1.3 Discussion

With quadratic tetrahedrons a minimum mesh density of 2 elements over thickness was found to be essential to capture both stiffness and prediction of state variables correctly. Refinement of the mesh up to three tetrahedrons through thickness yielded perfect convergence in stiffness but deviations in state variables still remained. Due to computational resources, an even higher mesh density was not considered relevant for practical applications and was therefore not tested for tetrahedrons.
Refining the shell mesh leads inevitably to aspect ratios that do no longer sufficiently satisfy the condition of thinness. In castings where the thickness of the wall is not necessarily small compared to other dimensions, this requirement limits the minimum size of the thin shell mesh. Compared to the increasing error in force-deflection the loss of accuracy of thin shells due to disproportionate mesh refinement was rather serious with respect to plastic strains and failure risks.

3.2 Generic fracture specimen

3.2.1 Motivation

In all three physical component tests the onset of fracture is found at the push out points on the bottom of the shocktower (shown in Fig. 14, section 4.4).
The crack initiates at the transition from the thick points to the less thick ribs. The discretisation of complex joints with thin shells is on the one hand often not unique, and on the other hand geometric simplifications made are not sensible. Moreover, the assumption of a plane stress state is certainly not justified, particularly in the notch base of the transition zone. It is to be checked whether both element types, shells and tetrahedrons, are able to predict failure under a complex stress state in a practical geometry derived from the tested component. Thus a quantitative conclusion can be drawn on the element performance concerning failure prediction. The reduced size of the generic specimen allows for a convenient study of the problem without simplifying it inadmissibly. At the same time a more detailed study of several discretisations is possible than the size of the full shocktower model would admit.

3.2.2 Modelling

The geometry of the specimen, Fig. 5, is derived from a section of the shocktower's bottom. To obtain a defined failure behaviour on one side of the push out point, two adjacent ribs are on one side of the push out point and only one rib on the other side, thus forming the weaker side.

© 2013 Copyright by Arup

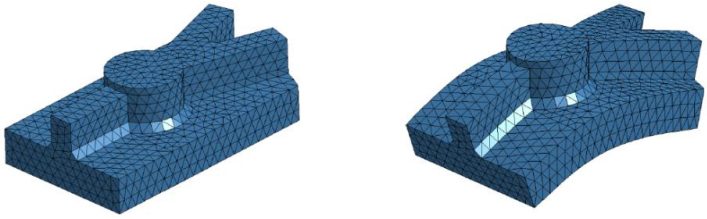

Fig. 5: Generic fracture specimen (undeformed / deformed configuration)

Besides two tetrahedron models with two and three elements through thickness different shell meshes are used. In addition to the standard 5 mm shell mesh, element sizes of 1 and 2 mm are used. At the same time the influence of the geometric detail is studied in the shell model, Fig. 6. It is once taken into account and once neglected for the medium mesh size.

While solid elements are able to represent the material accumulation in the cross section of the joint correctly, shell elements do not account for this stiffening effect.
In load cases where the rib is bended, scaling the shell elements' thickness in the joint can correct the lack of stiffness. In this case, the loading of the generic fracture specimen does not provoke a bending of the ribs but a stretching. Therefore, scaling the mentioned elements' thickness should not be necessary but it is to be checked whether a thickness scaling yields an overstiff behaviour in this load case. The scaling of the elements' thickness in the joint is performed only for the coarse mesh in order to check the achieved improvement or degradation. The element formulation of choice is the underintegrated type 2 with 5 integration points over the thickness. To estimate the influence of the integration point location, additionally the fully integrated shell element type 16 with four in-plane integration points is studied in one of the models.
The boundary conditions are applied to the ends of the specimen introducing a prescribed rotation around the centre of the geometry, Fig. 5. All specimens are put under plane strain condition to account for the out of plane dimensions in the shocktower.
For comparing the stiffness of the different discretisations, a cross section that yields the bending moment is defined next to the weak side of the push out point. To evaluate the failure prediction, the corresponding state variables in the critical element are regarded, Fig. 6.

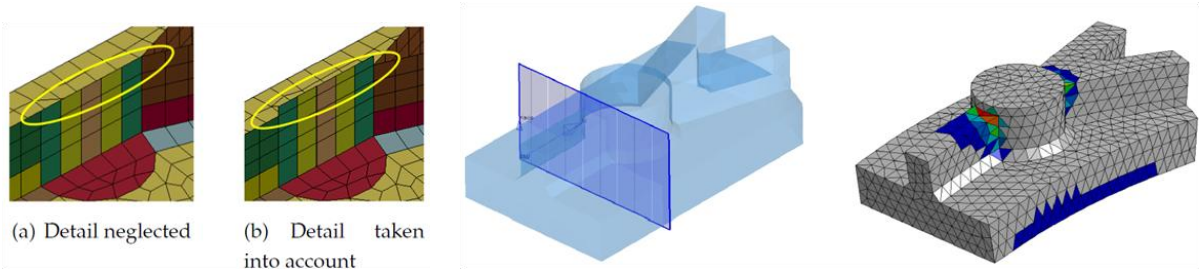

Fig. 6: Geometric detail in thin shell model (left ones), cross section in generic fracture specimen (middle) and critical elements in fillet (red contour, right)

3.2.3 Results

The two tetrahedron discretisations show perfect convergence in stiffness. In contrast, all shell meshed models yield a softer behaviour, the bending moment being approximately 10 % lower in the range of interest. Whereas the mesh size shows almost no influence on the stiffness, scaling the elements' thickness in the joint elevates the force a little. However, the change becomes significant only at higher loads at which the tetrahedron models have already failed, Fig. 7.

© 2013 Copyright by Arup

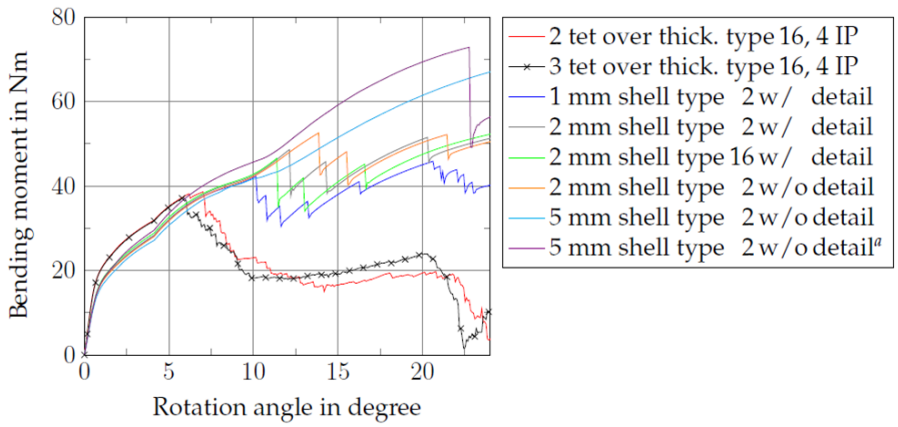

Fig. 7: Elastoplastic stiffness of generic fracture specimen

The bending leads to tensile stresses at the top of the rib which is the location that is critical in the shocktower as well. All models are able to indicate an elevated failure risk at the same element. However, very large quantitative differences between shell and tetrahedron discretisations are obtained in fracture prediction. In the specimen with three tetrahedrons over thickness fracture occurs at 5.8 deg. Shortly after that, at 6.2 deg, the coarser tetrahedron model with two elements through thickness predicts failure. The mesh size dependency is much larger for the shell elements, where the 1 mm shell mesh fails at 10 deg, while the coarse 5 mm specimen with unscaled thickness does not fail until the maximum loading at 24 deg. Between these bounds lie the results of the 2 mm mesh which again depend on the element formulation and the geometric representation, that is whether the detail on the push out point is regarded or not. If it is taken into account failure occurs at 12 deg while neglecting it leads to failure at 14 deg. Changing the element formulation to the fully integrated type 16 causes the specimen to fail at 11 deg, 1 deg earlier than with the underintegrated type 2 formulation. Just as scaling the element thickness does not alter the stiffness before higher bending radii, the failure risk is only elevated for higher loads and still far from the tetrahedron values, Fig. 8.
In contrast to the solid models, in all shell models instability is the critical failure mechanism, not ductile normal fracture whose risk does not exceed approximately 0.8 before failure occurs. As solids are able to model localised necking, no risk for instability is calculated.

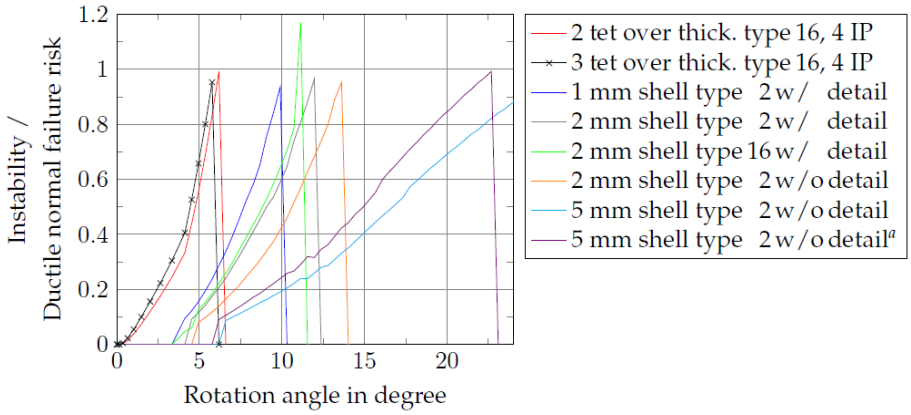

Fig. 8: Failure risk in generic fracture specimen at the critical location

The equivalent plastic strains deviate not only significantly between solid and shell models but also between the different shell models themselves, Fig. 9. While the 1 mm shell mesh predicts the same evolution of plastic strain as the hexahedron models do, all other shell models yield a lower increase. Nevertheless, the maximum plastic strains of about 19 % that are reached before failure are much higher in shell models than in hexahedron specimen (~5 %).

© 2013 Copyright by Arup

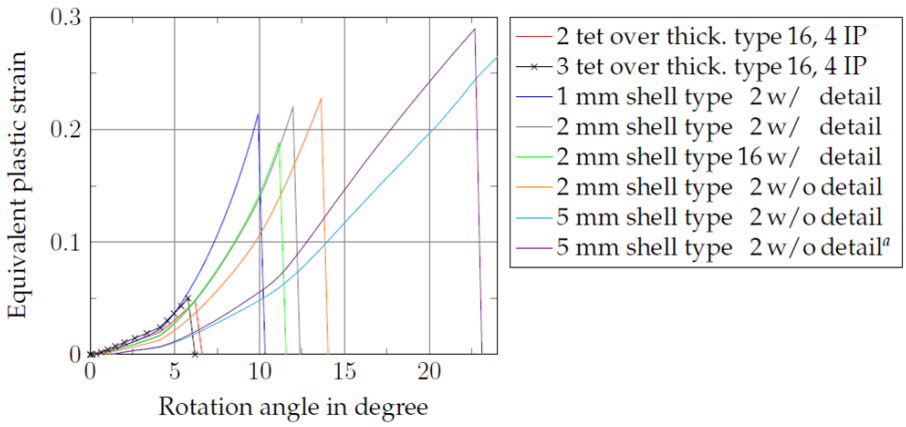

Fig. 9: Equivalent plastic strain in generic fracture specimen at the critical location

The stress triaxiality remains almost constant in the critical element in each of the shell models and is considerably lower than in the tetrahedron models. In the latter ones the triaxiality increases from a value of 1.0 to ~1.3 and ~1.6, respectively, Fig. 10.

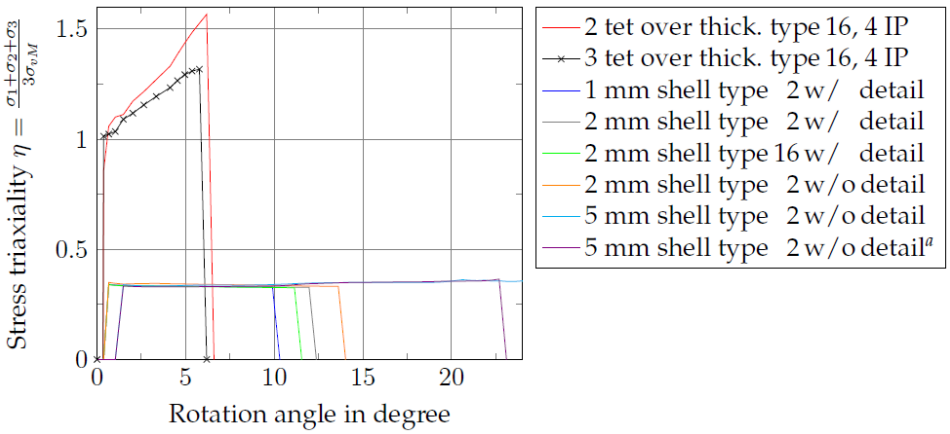

Fig. 10: Stress triaxiality in generic fracture specimen at the critical location

3.2.4 Discussion

The generic fracture specimen clearly shows the superior fracture prediction of tetrahedrons compared to shell elements. The failure risk is strongly underestimated by all thin shell models and moreover depends critically on the element size. This dependency is considered crucial as no convergent solution can be expected if the mesh is continuously refined for specific loading conditions, which has been shown in the buckling test where erroneous results are obtained for badly shaped shells. In the area of the rib – due to the orientation of the shells – the position of the integration points is not suited to capture the occurring gradients well. Using fully integrated shell elements improves the fracture prediction slightly, yet the deviations from the tetrahedron results remain very large.
The comparison of the triaxiality shows that all shell discretisations yield pure tension, while the triaxiality in the tetrahedron models is considerably higher which is what can be expected due to the stress concentration in the fillet.
Besides the revealed shortcomings of fracture prediction in the shell specimens, the issue of meshing V-joints becomes obvious. It is not unique where the midsurfaces of the two ribs join inside the push out point. For these reasons shell elements are not suited to predict failure in castings precisely.

© 2013 Copyright by Arup

4 Finite element analyses of automotive component

4.1 Motivation

The previous studies revealed large deviations in both elastoplastic stiffness and especially in fracture prediction for different element types, formulations and mesh sizes. However, these deviations also depend on the loading conditions.
For this reason the effect of discretisation and element formulation needs to be studied in a practical component where some of the specific shortcomings and benefits may be more or less pronounced than in the basic studies with idealised geometries and boundary conditions. Moreover, this allows not only for a comparison between different finite element simulations but also for a quantitative assessment with regard to experimental results.

4.2 Modelling

In the testing assembly, Fig. 11, all parts but the shocktower are supposed to be purely elastic, using standard properties of steel. Screws and bolts are modelled as beams, connecting the different parts via constrained node sets. No stress initialisation to simulate tightened screws is performed. As the drill holes are not modelled in the FE-model, the nodes located in these areas are directly connected to their respective beams. In addition to the standard shell meshes and coarse tetrahedron mesh used by JLR for crashworthiness simulation, a refined tetrahedron mesh is used. It is based on the regular tetrahedron mesh, but a python script is used to split each element of the shocktower into 12 quadratic subtetrahedrons. By this procedure a minimum of two elements over thickness is guaranteed all over the shocktower which is found to be essential for fracture prediction in the previous basic studies. Besides the force-deflection curve that can directly be compared to the real test results, the plastic strain distribution is considered as well. Particularly at the bottom of the shocktower, where failure occurs in the test, a qualitative and quantitative comparison between the different discretisations and the test results is performed.

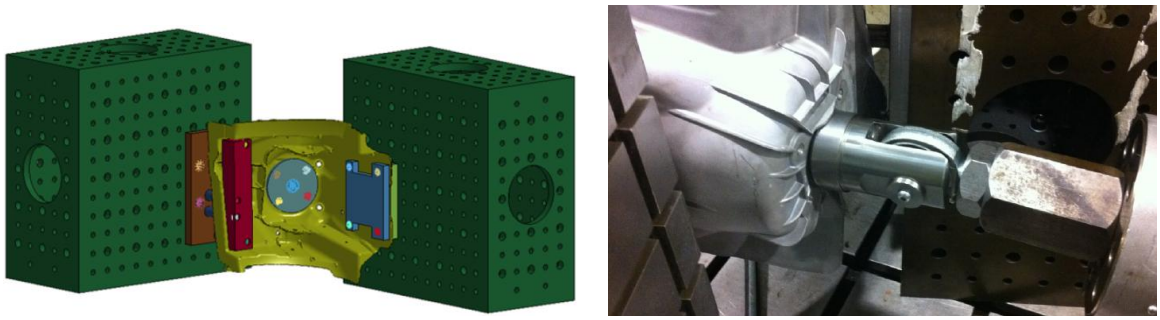

Fig. 11: FE-model of shocktower testing assembly (left) and view at bottom of shocktower, mounted in testing assembly

4.3 Results

The elastic stiffness shows good convergence between shell and solid discretisations, Fig. 12. Only the 10 mm shell mesh yields already a slightly stiffer elastic response than the other models. For larger displacements the deviations between shell and tetrahedron models become larger, both tetrahedron results lying close together between the stiff 10 mm shell mesh and the soft 5 mm shell mesh. While the latter ones yield very smooth force-deflection curves, both solid model results show small discontinuities in their response. Particularly in the split tetrahedron mesh where some elements at the inside of the shocktower reach their fracture limits already at a low loading level, element deletion leads to the observed discontinuities.
The first model that fractures is the 5 mm shell model at a load of 170 kN and a displacement of 11.8 mm. Shortly after that (0.5 mm) the split tetrahedron model fails under a load of 176 kN. It is followed by the coarser solid model at 183 kN and a displacement of 12.6 mm. Finally the coarse shell mesh fails at 236 kN and 18.4 mm displacement. It is the only one that deviates significantly in the maximum force that is predicted.

© 2013 Copyright by Arup

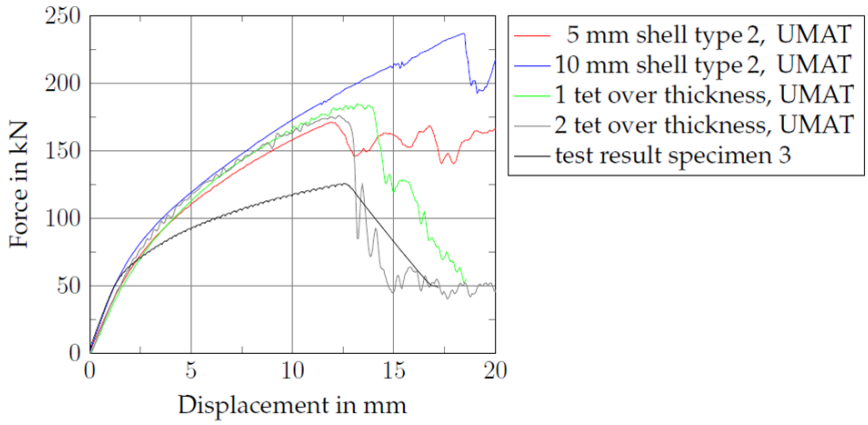

Fig. 12: Force-deflection curve of finite element analyses compared with experimental test results

Although the drop in force is relatively small between the fine shell mesh and solid results, the location of crack initiation differs remarkably. Independently from the mesh size itself, both tetrahedron meshes yield first failure at one of the push out points, Fig. 13. In contrast to that, the shell models predict failure at a joint in the outer region, not directly in the area where the shocktower is loaded. When the critical areas of the shell models are compared with the corresponding areas of the tetrahedron models it is found that the tetrahedron models predict failure at push out points and an elevated risk at two distant ribs (no fracture in tests, but might be highly stressed).
On the other hand the shell models predict failure at one of these ribs but not at push out points or their directly adjacent ribs (not even elevated risk).

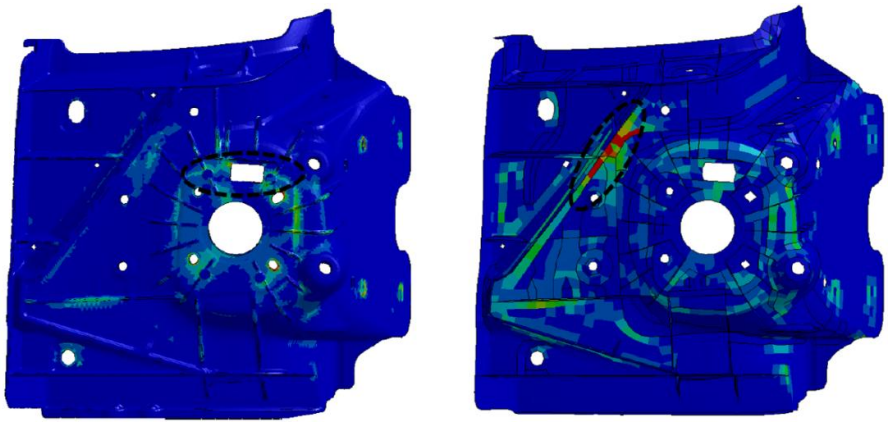

Fig. 13: Critical locations at bottom of shocktower solid (left) and 5 mm shell (right) model

4.4 Discussion and correlation with tests

The analyses under simplified conditions reveal the overstiff behaviour of the coarse shell mesh which is not able to represent all deformation modes properly. Regarding the geometric discretisations such as drill holes and fillets as well, the 10 mm mesh proves to be inappropriate to model the details of this shocktower. Even if in some areas the aspect ratio of the shells might not be suitable, the finer mesh seems to be a reasonable compromise between an accurate geometric representation and the demand to keep the elements thin enough to serve their original purpose. This is also confirmed by the fact that the 5 mm shell mesh shows only a negligible deviation in stiffness compared to the tetrahedron model.
A noticeable difference between the fully and underintegrated shell elements can be observed for both mesh densities which suggests to use the underintegrated shells in conjunction with a reasonable hourglass control as a quantification of the shear locking effect or a reliable estimation is in general not possible.
Regarding the influence of T-joints in this test, the small deviation in the elastoplastic behaviour between the 5 mm shell mesh and the tetrahedron mesh indicates that there is no compelling need to

© 2013 Copyright by Arup

modify the shell thickness in joint areas. In this test, the T-joints of the component are mostly stressed under tensile or compressive loads but not under bending. However, applying different loading conditions on this shocktower may show a need to alleviate the low stiffness of shell meshed T-joints.
Though the physical stiffness is slightly higher than the one obtained by the fine shell and the two tetrahedron models, the accordance of the analyses and the corresponding experimental results is good, Fig. 12. However, at higher loads there is a large deviation between the force-displacement curve of the test and the ones attained by simulation. The deviation starts at a deflection of about 2.5 mm and increases up to rupture. None of the previous studies show crucial shortcomings in the characterisation and modelling of the material or of the discretisation with tetrahedrons. Taking into account that considerable slip occurred in all experimental tests, it seems to be a reasonable explanation that this effect is the main cause for the large deviations between simulations and experiment.
When fracture occurs and the force-displacement curves drop in the 5 mm shell model and the tetrahedron models, the experimental force-deflection curve also reports failure of the shocktower. However, if several millimetres of slip are already included in the physical curve, the failure prediction of all simulations is too late. The fact that there is still a considerable difference between the regular and the split tetrahedron mesh in the displacement where fracture occurs, indicates that no convergent solution has yet been given by the investigated discretisations.
With respect to the plastic strain distribution and the areas of elevated failure risk, the superior performance of solid modelling which was already found in section 3.2 is confirmed. Both tetrahedron models are able to predict the location of fracture initiation precisely, Fig. 14, and even accord well with the crack propagation observed in the tests, Fig. 15. In contrast to that, none of the shell models indicates an elevated failure risk in the area where the component fails. Moreover, another location is identified to be critical and finally fractures, thus unloading the bottom of the shocktower and eluding the fracture near the push out points.

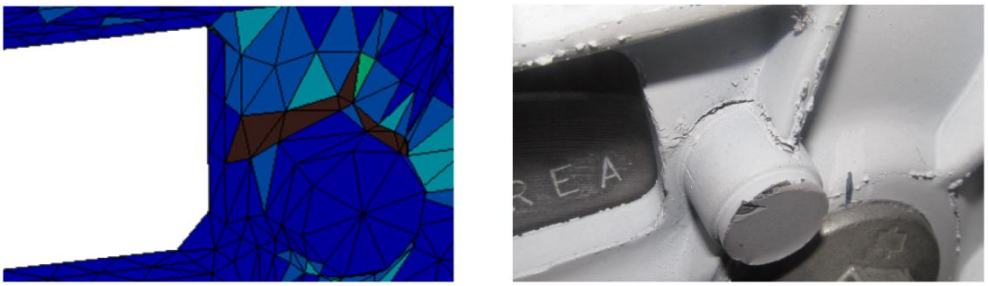

Fig. 14: Crack initiation in tetrahedron finite element model and real shocktower

Fig. 15: Crack propagation in tetrahedron finite element model and real shocktower

The shocktower test reveals the necessity to capture the geometry and the occurring stress states to allow for a qualitative fracture prediction. For accurate quantitative information on fracture a sufficiently fine solid mesh is essential to be able to represent the gradients in the component. As even the refined tetrahedron model with more than 2 million elements is not supposed to be a convergent solution, current limits of computational power that is spent on analyses of automotive components are reached. Nevertheless, as the critical spots are correctly identified, reliable data for improvements in design of components can be obtained by finite element computations if discretisation and material modelling are reasonable and physically correct.

© 2013 Copyright by Arup

5 Summary

Comparison of the results of different tetrahedron and shell meshes in the performed tests reveals the superior performance and higher reliability of solid elements. The capability of fracture prediction in geometries with complex stress states is found to be insufficient and strongly mesh dependent using thin shell elements.
Although between thin shells and solids a satisfying accordance in the elastoplastic range is found under testing conditions, significant deviations in fracture prediction are noted. Besides the fact that failure is predicted at a wrong location by both shell models, no elevated risk is yielded at the spots where cracks initiate in the experimental tests.
In contrast to that, both tetrahedron models give an accurate prognosis of the critical location in the shocktower. As already observed in the previous basic studies, the refinement of the tetrahedron mesh yields no more improvements in stiffness but in the quantitative prediction of fracture. However, global splitting of all tetrahedron elements increases the number of elements – and thus also the CPU-time – by a factor of 12. Hence, using the current resources in the industrial development process, only a qualitative but reliable finite element analyis of automotive castings with quadratic tetrahedrons and a physically motivated material model appears to be the most promising way to derive suggestions for improvement in design, construction and material selection.

6 Acknowledgment

The authors would like to thank Prof. Thomas Böhlke from the Karlsruhe Institute of Technology for his support and helpful suggestions for the diploma thesis, this paper is based on.

7 Literature

[1] Dell, H., Gese, H. "Experimental and theoretical characterization of an aluminium HPDC alloy for crash simulation", 2012, Technical report of MATFEM on behalf of Jaguar Landrover

[2] Dell H., Gese H., Oberhofer, G.: "Advanced Yield Loci and Anisotropic Hardening in the Material Model MF GenYld + CrachFEM", Numisheet 2008, Interlaken, Switzerland

[4] Gese, H., Project on material characterization of an aluminium HPDC, Technical report of MATFEM, 2012

[5] Dell H., Gese H., Oberhofer, G.: "CrachFEM - A Comprehensive Approach for the Prediction of Sheet Metal Failure", Numiform 2007, Part I, AIP Conference Proceedings, American Institute of Physics (2007), 165–170

[6] Hooputra, H., et al., "A comprehensive failure model for crashworthiness simulation of aluminium extrusions", International Journal of Crashworthiness 9 (5), 449-464

© 2013 Copyright by Arup